Exciton migration in a polythiophene: Probing the spatial and energy domain by line-dipole Förster-type energy transfer

ARTICLE *in* THE JOURNAL OF CHEMICAL PHYSICS · APRIL 2005

Impact Factor: 2.95 · DOI: 10.1063/1.1855292 · Source: PubMed

Exciton migration in a polythiophene: Probing the spatial and energy domain by line-dipole Förster-type energy transfer

Sebastian Westenhoff,[a] Clément Daniel, and Richard H. Friend
Cavendish Laboratory, University of Cambridge, Madingley Road, Cambridge CH3 0HE, United Kingdom

Carlos Silva
Département de Physique, Université de Montréal, C.P. 6128, Succ. Centre-ville Montréal, Québec H3C 3J7, Canada

Villy Sundström and Arkady Yartsev
Department of Chemical Physics, Lund University, Box 124, S-221 00 Lund, Sweden

(Received 22 October 2004; accepted 9 December 2004; published online 24 February 2005)

We study exciton migration in low molecular weight poly[3-(2,5-dioctylphenyl)thiophene] in dilute solution by means of ultrafast spectroscopy and Monte Carlo simulations of resonance energy transfer using the line-dipole Förster approach. The model includes the build-up of polymer chains, site-selective exciton generation, and diffusion through incoherent energy transfer. Time-resolved, ensemble-averaged experimental data are reproduced, namely photoluminescence spectral migration and stimulated emission anisotropy decays measured by streak camera and femtosecond transient absorption spectroscopy under site-selective excitation conditions. Importantly, the relatively simple line-dipole Förster-type approach beyond the point-dipole approximation reproduces both experiments quantitatively. Since explicit chain conformations are used in the model, the simulations yield a descriptive microscopic picture of exciton migration. The effective conjugation length ($l_{seg}=2.9$ nm, 7.4 monomer units) and the disorder of the chains ($\Omega=0.8$) are yielded as the only fitting parameters. We find an extra component that is not covered by our fits in anisotropy decays at early times for high excitation energies. This is interpreted within the context that the effective conjugation is limited by conformational disorder. © *2005 American Institute of Physics*. [DOI: 10.1063/1.1855292]

I. INTRODUCTION

Semiconductor polymers are an exciting class of materials that is finding applications as light-emitting diodes,[1] photovoltaic devices,[2] and field-effect transistors.[3] Owing to their solubility in organic solvents, they are easily processable, e.g., by ink-jet printing.[4,5] Essential for technical application of this class of materials is that excitons and charges can migrate along and between chains. For example, exciton migration (also referred to as exciton hopping or exciton transport) is essential for the efficient operation of polymer-based photovoltaic devices in which the sunlight is harvested in the bulk polymer and transported to an interface with a charge accepting material where efficient charge separation occurs.[2,6]

In polymeric semiconductors, the main transfer mechanism of exciton migration is resonance energy transfer (RET) between weakly coupled chromophores.[7] Disorder leads to a distribution of the energy of these conjugated segments and thus to inhomogeneous broadening of the $\pi-\pi^*$ absorption band at room temperature.[8] Structurally, the chromophores are thought to be a part of the chain where (at least) the S_1 excited state is electronically separated from the remaining electronic system.[9] The length of these segments is important because it relates to the extent of effective conjugation. This modulates the energies of the electronic ground- and excited states, and also the extent of the electronic wave functions.[10] Importantly, the energy of the $\pi-\pi^*$ transition is inversely proportional to the effective conjugation length associated with each conjugated segment. There are several sources for the break of conjugation along the polymer backbone. The "wormlike" model is based on breaks arising as a consequence of fast fluctuations of electronic oscillators.[11,12] Another source is that conformational disorder or structural faults cause the distribution of conjugation lengths.[13] In the case of oligothiophenes, quantum-chemical calculations explicitly show that conformational disorder due to chemical defects, kinks, bends, and twists causes breakup of the conjugation along the chain.[14] Furthermore, interchain contact modulates the energy of the $\pi-\pi^*$ transition in films[15] and isolated chains bending onto itself.[16] Energetic and conformational disorder are intimately interconnected with exciton migration because they lead to a broad distribution of RET rates between conjugated segments.

Experimental evidence for RET is mainly found in two optical experiments: site-selective photoluminescence (PL) spectroscopy[17–21] and time-resolved polarization anisotropy measurements.[22–24] Low-temperature, site-selective steady-state PL spectra[17,18] reveal that the peak position depends on the excitation energy for energies approaching the red edge of the absorption band. Thus, in case of low temperatures, there exists an localization energy below which the excitons

[a]Electronic mail: sw372@cam.ac.uk

are effectively immobilized during their lifetime because of a lack of low-energy acceptor sites in their neighborhood.[17] In time-resolved site-selective PL spectra of a poly(*p*-phenylenevinylene) (PPV) derivative,[19] the PL shifts bathochromically and is narrowed due to incoherent energy hopping. Excitons transfer to neighboring conjugated segments preferably downhill in energy, whereas uphill energy transfer is significantly slower as it is thermally activated.

Conformational disorder can be observed in ultrafast polarization anisotropy experiments. In polythiophenes and PPV derivatives, the randomization of polarization has been shown to be due to exciton migration along[22] and between[23,24] structurally disordered chains on femtosecond and picosecond time scales. Grage *et al.* use Monte Carlo simulations of RET on conformationally disordered chains to model femtosecond time-resolved anisotropy.[22–24]

We note that primary photoexcitations undergo vibronic cooling leading to exciton self-localization (also referred to as polaron-exciton).[14,17,23] This process is expected to occur on a time scale faster than 100 fs due to its coupling to phonons. For films of another polythiophene derivative it was determined to be 37 fs.[24] Since our measurements are not sensitive on such short time scales, and we do not see a big effect on the initial anisotropy, we neglect it in the simulations.

A number of papers were published that are devoted to finding an analytical solution of the dissipative exciton transport on strongly disordered chromophores.[25–27] However, even though the theory has produced considerable insight into the fundamental physical process, application to exciton migration in conjugated polymers has been rare, and in a recent publication it was shown that this approach cannot be used to fit ultrafast anisotropy data satisfactorily.[28]

As an additional transport process, dynamic conformational disorder may contribute to exciton migration directly.[29,30] In these simulations, conformational defects undergo spatial and temporal fluctuations leading to superimposed exciton migration by dynamic conformational disorder and RET. Challenging the RET model are reports of a polyfluorene[31] and a poly(*p*-phenylenethynylene)[32] derivative in which the authors propose that spectral relaxation and line narrowing are caused by fast planarization of the excited conjugated segments.

In this report we will work within the framework of the established RET model. The first question that motivates the investigation is to relate the energetic perspective of RET to a realistic structural picture of chain conformations. Is it possible to quantitatively apply Monte Carlo simulations based on a modified Förster-type model to describe RET of excitons on chains with realistic length scales and use this to get a detailed microscopic picture of excitons hopping along the chains? We obtain quantitative information about the length of the chromophores (which equals the effective conjugation length), trapping mechanism, and hopping time scales. Our second objective is to investigate if RET is the only underlying physical process influencing anisotropy decay and spectral relaxation. Can we identify if additional processes play a role for exciton migration?

For the investigations, we use low molecular weight (M_W=70000 g/mol) poly[3-(2,5-dioctylphenyl)thiophene] (PDOPT) in dilute chloroform solution (see the inset of Fig. 2 for chemical structure), which is a model polymer for RET.[22] The bulky sidechains of the polymer reduce interchain coupling, resulting in high PL quantum yields of 0.37 and 0.24 in solutions and films, respectively.[33] Dilute solutions of relatively short chains are convenient for our purpose, because the chains are spatially well separated so that energy transfer occurs along the backbone only, and it is reasonable to neglect the formation of intrachain species.

We use a Monte Carlo simulation of line-dipole Förster energy transfer to model time-resolved PL spectral shift and anisotropy experiments under site-selective excitation conditions. The use of the line-dipole approximation is necessary because the point-dipole approximation used in the traditional Förster theory does not hold for short transfer distances between extended dipoles as in polymers.[34] The advantage of the line-dipole concept is that with moderate computational effort the simplicity and flexibility of the Förster equation is retained, while the accuracy is increased by at least an order of magnitude over the point-dipole approximation.[35] We present a formalism to calculate the transfer rate with parameters that are experimentally available only. The generation of chain conformations uses two fitting parameters. The disorder parameter (Ω) reflects the conformational disorder of the chains, and l_{seg} is the center of the distribution of chromophore lengths. l_{seg} and Ω can be fitted independently to the dynamic redshift of the PL and anisotropy values at long time delays after photoexcitation, respectively.

II. EXPERIMENT

Samples of PDOPT (Ref. 36) were prepared by dissolving the polymer in chloroform to obtain a optical density of $\sim$0.2 at the excitation wavelength in a 1 mm cuvette. The optical density was chosen to assure homogeneous excitation throughout the sample. For femtosecond transient absorption (FTA) measurements we used a Clark MXR CPA-2001 that produces light pulses of 150 fs at 775 nm with 1 kHz repetition rate. The pump and probe wavelengths were tuned by two noncollinear optical paramagnetic amplifiers (NOPA) without pulse compression.[37] The polarization of the pump beam was set to 45 deg to that of the probe beam at the sample position. We used a Berek compensator to optimize the pump polarization to a contrast ratio of $<10^{-3}$. The probe pulses were separated into parallel and perpendicular parts by a Glan polarizer after passing through the sample. In order to achieve a contrast ratio of $<10^{-5}$, we passed the separated parts of the beam through two additional Glan polarizers before detection by two Si photodetectors. This detection scheme has a high intrinsic signal-to-noise ratio for anisotropy data, because laser pulse fluctuations are excluded as noise source. We tested the setup with a solution of Rhodamine 6G, where the initial anisotropy was found to be 0.4. In order to avoid any artifacts from the overlap of pump and probe, the initial 150 fs of the anisotropy data were ne-

glected in the analysis. The anisotropy and population dynamics were tested to be insensitive to the intensity of the probe beam.

Picosecond time-resolved PL measurements were carried out using a streak camera (Hamamatsu C 4742-95). A Tsunami oscillator (pumped by a Millenia X) produced 100 fs pulses at 82 MHz. An optical paramagnetic amplifier (OPAL, Spectra Physics) and sum frequency generation were used to tune the pump wavelengths. The response function was 1.5 ps. Polarization of the pump was set to be magic angle (54.7 deg) with respect to that of the detected fluorescence. The data were corrected for chirp, and spatial and spectral sensitivity of the streak camera. In both experiments the pump power was tested to be below the threshold for bimolecular annihilation processes.

III. SIMULATIONS

Each Monte Carlo loop consisted of two stages: (i) generation of the polymer chain and population of excitons and (ii) a time evolution loop where the exciton migrates through RET. Typically, we averaged over 20 000 to 200 000 Monte Carlo loops (5000 to 50 000 excitons) to obtain reasonable statistics.

Following the method published by Grage *et al.*, the polymer chain was built from a succession of conjugated segments represented as vectors in line with the chain.[14,22] The conformational disorder was introduced by displacing each vector with respect to the previous one

$$\mathbf{t}_{i+1} = \mathbf{t}_i + \mathbf{t}_D. \tag{1}$$

$\mathbf{t}_i$ are the normalized vectors that constitute the polymer chain and $\mathbf{t}_D$ consists of three random numbers taken from a Gaussian distribution with standard deviation Ω. This parameter will be referred to as the disorder parameter. In order to account for the distribution of molecular weights, the chain-lengths were allowed to vary following a Gaussian distribution with mean of 17 and standard deviation of 3 conjugated segments. In addition to that, the chain was prevented from bending onto itself by setting the minimum distance for any two points in the polymer chain to 4 Å in agreement with size exclusion chromatography measurements of thick PDOPT films.[38]

Beyond Grage's approach, each segment was assigned an energy that was inversely proportional to its length, l_{seg}.[39] The distribution of energies was assumed to be the inhomogeneous line shape of the absorption spectrum. In order to estimate the inhomogeneous (σ_{inh}) and homogeneous linewidth (σ_{hom}), time-integrated absorption and PL spectra were fitted with the sum of three equally spaced Gaussians with standard deviation, σ_{tot}. Both line shapes were assumed to be Gaussian so that the following relation holds:

$$\sigma_{\mathrm{tot}}^2 = \sigma_{\mathrm{hom}}^2 + \sigma_{\mathrm{inh}}^2. \tag{2}$$

The RET transfer rate and thus the spectral overlap [see Eq. (5) below] should satisfy the detailed balance principle by following a Boltzmann distribution

$$\frac{I_{E_1 \to E_2}}{I_{E_2 \to E_1}} = e^{-\Delta E/kT}. \tag{3}$$

$I_{E_1 \to E_2, E_2 \to E_1}$ is the spectral overlap, whereas E_1 and E_2 denote the energy of two chromophores, ΔE is the difference between E_1 and E_2, k denotes the Boltzmann constant, and T is the temperature. In a cyclic procedure, σ_{hom} and σ_{inh} were estimated by testing the spectral overlap against the Boltzmann distribution to yield room temperature and visually judging the fits. A region spanning from $\sigma_{\mathrm{inh}} = 71$ meV to $\sigma_{\mathrm{inh}} = 94$ meV was found to give acceptable fits. This agrees well with finding for conjugated polymers by other groups.[40,41] The center of the Gaussian for the first vibrational peak in the photoluminescence (absorption) was 2.14 eV (2.33 eV), and the spacing between the three Gaussians representing the vibrational progression was 0.178 eV.

During the initial placement of excitations, the homogeneously broadened line shape of each segment and its orientation were taken into account

$$P_i = A_{\mathrm{ex}}(\mathbf{t}_i \,.\, \mathbf{z})^2 \varepsilon(E_{\mathrm{laser}} - E_i), \tag{4}$$

where A_{ex} is a constant proportional to the excitation fluence, i counts the segments, $\mathbf{t}_i$ is the normalized orientation vector of the segment, $\mathbf{z}$ is the normalized orientation vector of the excitation polarization, $\epsilon(E)$ is the homogeneous absorption line shape, E_{laser} is the excitation photon energy, and E_i is the chromophore energy.

Fermi's golden rule describes incoherent energy transfer in the limit of weak coupling from donor D to acceptor A

$$k_{DA} = \frac{2\pi}{\hbar} I_{DA} V_{DA}^2. \tag{5}$$

I_{DA} is the spectral overlap and V_{DA} is the Coulomb coupling between donor and acceptor, which we estimate from line-dipole approximation.[35] In this approach, the conjugated segments are divided into a number of subsegments, denoted as k and l for donor and acceptor, respectively. The Coulomb integral for transition from D to A is calculated as

$$V_{DA} \propto \sum_{k,l}^{l_d} \Psi_k |\kappa_{kl}| R_{kl}^{-3} \Psi_l, \tag{6}$$

$$\Psi_k = \frac{\sin \dfrac{\pi k}{l_d + 1}}{\sum_a \sin \dfrac{\pi a}{l_d + 1}}. \tag{7}$$

$\Psi_{l,k}$ is the center of mass excitonic wave function representing a point particle in a finite 1D space with no boundary conditions as described by Beenken and Pullerits, who also give a detailed derivation of Eq. (6).[35] The number of subsegments (l_d) was set to 6. We computed Coulomb integrals (V_{DA}) between adjacent conjugated segments with in-line configuration for several values of l_d and found that $l_d = 6$ was close to the asymptotic value of V_{DA} (for high values of l_d) and that the computing time is reasonably small (see below Fig. 7). We note that Eq. (6) becomes the point-dipole approximation for $l_d = 1$. κ_{kl} is a factor accounting for the

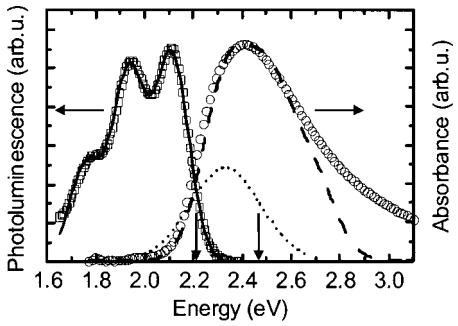

FIG. 1. Time-integrated PL and absorption spectra of PDOPT in chloroform solution. The open squares and the open circles denote the experimental PL and absorption, respectively. The excitation wavelength was 2.47 eV. The solid and dashed line are fits as described in the text. The vertical arrows mark the excitation wavelength for the time-resolved experiments, and the dotted line is the inhomogeneously broadened DOS used in the simulations with $\sigma_{\mathrm{inh}}=71$ meV. The associated homogeneous broadening was $\sigma_{\mathrm{hom}}=60$ meV.

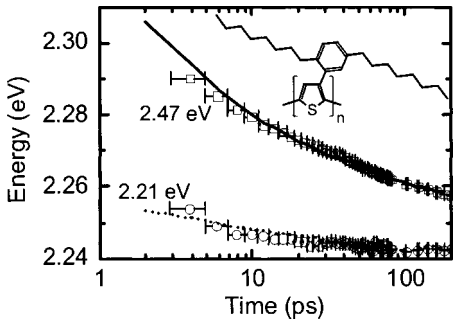

FIG. 2. Average energy of segments occupied by excitons plotted versus time after photoexcitation for PDOPT in chloroform solution. The solid and dashed line represent the modeled data for 2.47 and 2.21 eV excitation energies, respectively. The experimental values, shown as open squares (excitation at 2.47 eV) and circles (excitation at 2.21 eV), are integrated spectra (spectral window: 1.88 to 2.25 eV and 2.05 to 2.50 eV for the two excitation energies, respectively; time window: 2 ps). The experimental graphs are shifted arbitrarily to overlap with fits at late times and the error bars indicate the width of the time window. The inset shows the chemical structure of PDOPT.

orientation of the subsegments and R_{kl} is the distance between the centers of the two subdipoles k and l. κ_{kl} is given by the following relation:[42]

$$\kappa_{kl}=(\mathbf{t}_k\cdot\mathbf{t}_1)-3(\mathbf{t}_k\cdot\mathbf{R}_{kl})(\mathbf{t}_1\cdot\mathbf{R}_{kl}). \tag{8}$$

The normalized vectors $\mathbf{t}_{k,l}$ denote the orientations of subsegments k and l. $\mathbf{R}_{kl}$ is the vector connecting their centers. By replacing κ and R^{-3} terms in the usual Förster deviation[42] with the sum from Eq. (6), we arrive at the modified line-dipole Förster equation

$$k_{DA}^{LR}=\frac{1}{\tau_D}\frac{9000\ln(10)\Phi_D}{128\pi^5 N n_{\mathrm{solv}}^4}I_{DA}\left[\sum_{k,l}^{l_d}\Psi_k|\kappa_{kl}|R_{kl}^{-3}\Psi_l\right]^2. \tag{9}$$

τ_D represents the lifetime of the donor site (583 ps, taken to be the lifetime of the magic angle stimulated emission decay as measured by FTA), Φ_D is the quantum yield of PL of the donor site and was reported earlier to be 0.37,[33] N is Avogadro's number, and n_{solv} is the refractive index of the solvent (1.446 for chloroform). I_{DA} is the spectral overlap of the homogeneously broadened spectra of the segments D and A.

The random walk of the exciton on the polymer chain was followed by the average energy of all excited segments and by the ensemble averaged anisotropy

$$r(t)=\frac{\sum_i(\mathbf{t}_i\cdot\mathbf{z})^2-\sum_i(\mathbf{t}_i\cdot\mathbf{x})^2}{\sum_i(\mathbf{t}_i\cdot\mathbf{z})^2+2\sum_i(\mathbf{t}_i\cdot\mathbf{x})^2}. \tag{10}$$

The normalized orientation vector is denoted by $\mathbf{t}_i$, $\mathbf{z}$ is the direction of excitation polarization, and $\mathbf{x}$ is a reference vector perpendicular to it.

IV. RESULTS

The time-integrated optical spectra and fits for PDOPT in dilute chloroform solution are presented in Fig. 1. The density of states (DOS) used in the simulations is shown for comparison as the dotted line. The vertical arrows mark the excitation energies used in the time-resolved experiments. The fits (solid and dashed line) were obtained by following the procedure outlined in Sec. III. Since we take only the first electronic excited state with three vibronic transitions into account (sum of three Gaussians), the blue edge of the absorption is not well reproduced. However, for placement of the excitons and computation of the spectral overlap, this region is not important and hence it is reasonable to neglect higher vibronic peaks.

Figure 2 shows the experimental (data points) and simulated (continuous line) spectral shifts for the two excitation energies, 2.47 and 2.21 eV. In case of the simulated data points, the y axis is the mean energy of all excited segments. For the experimental values it represents the center energy of the spectral window integrated over 2 ps

$$\overline{E}=\frac{\sum_i^n E_i I_i}{\sum_i^n I_i}. \tag{11}$$

$\overline{E}$ is the center energy, n the number of data points, and E_i and I_i are the energy and PL intensity at each data point, respectively.

Essentially, both excitation energies can be fitted with the same fitting parameters: $l_{\mathrm{seg}}=2.9$ nm, and $\Omega=0.8$. We note that $\Omega=0.8$ was determined by the fits shown in Fig. 3. The broadenings were derived from steady-state spectra as described above ($\sigma_{\mathrm{inh}}=71$ meV and $\sigma_{\mathrm{hom}}=60$ meV). Excitation at the peak of the $\pi-\pi^*$ transition absorption band (2.47 eV) results in a redshift of ~60 meV, whereas excitation at the red edge of the absorption (2.21 eV) yields a smaller redshift of ~10 meV. Limited by the time resolution of 1 ps and the width of the time window, the experimental data points show a smaller overall redshift. However, the excitation migration is sufficiently slow for the experiment to catch 50% of the overall energy shift, and a good fit can be obtained. The difference in the energies at long times can be explained by the fact that each polymer chain has a limited number of chromophores (around 17). During its progression on the chains the exciton will not find the lowest energy sites of the DOS, but rather the one which is available on the

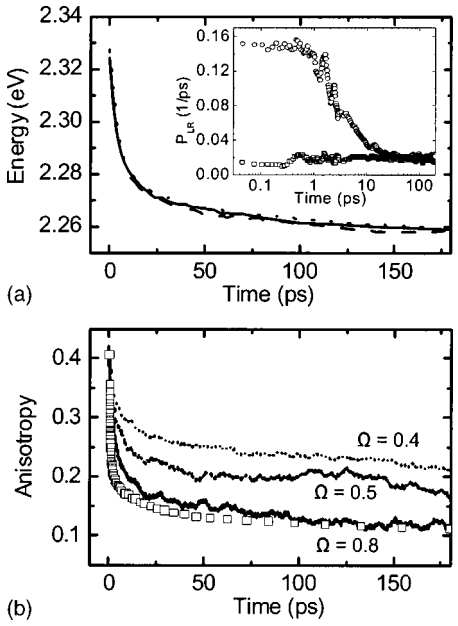

FIG. 3. Influence of the disorder parameter Ω. (a) Simulated average exciton energy and (b) polarization anisotropy (FTA, detection at 1.96 eV) of PDOPT dissolved in chloroform for three disorder parameters Ω=0.8 (solid line), Ω=0.5 (dashed line), and Ω=0.4 (dotted line). Excitation energy was 2.47 eV and l_{seg}=2.9 nm for all traces. The experimental anisotropy is shown as open squares in panel (b). The inset in panel (a) shows the probability for an exciton to transfer up (open squares) and down (open circles) in energy.

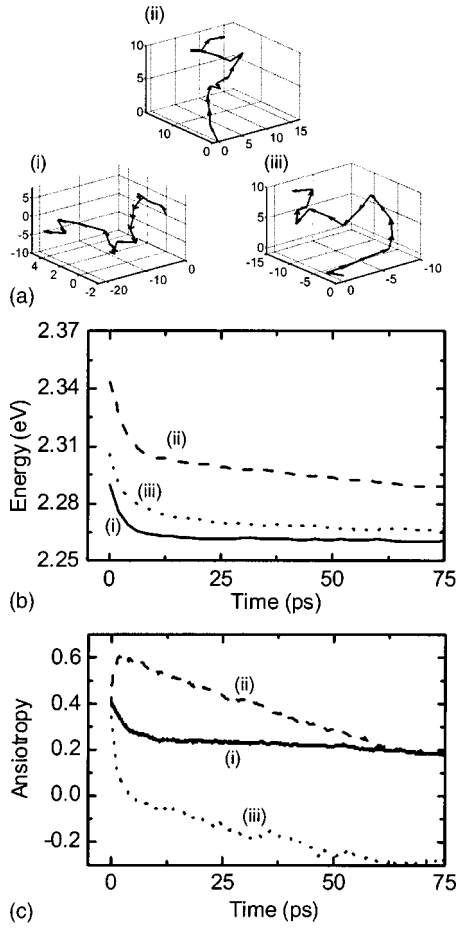

FIG. 4. Panel (a) shows three randomly generated polymer chain configurations with disorder factor Ω=0.8. Panel (b) and panel (c) show the spectral migration and anisotropy decay averaged over 2500 excitons for chain conformation (i) solid line; (ii) dashed line; and (iii) dotted line.

particular polymer chain. Since excitation with low energies will preferentially excite low-energy segments and thus preselect chains that have a low-energy chromophore available, the difference becomes understandable. The effective conjugation length of l_{seg}=2.9 nm corresponds to 7.4 monomer units. By comparison to oligomer spectra, the length of a conjugated segment in PDOPT was estimated to be around 6 monomers.[22] This shows that the line-dipole approximation can quantitatively explain spectral migration by incoherent energy transfer.

In an earlier work it was reported that anisotropy is a measure for disorder of polymer chains.[22] The crucial parameter is the disorder parameter Ω, which is examined in Fig. 3. We recall that Ω determines the disorder in the polymer chains and the exciton hopping is affected subsequently. Here, l_{seg} was not adjusted to fit the anisotropy decay but was rather left constant from the best fit of spectral migration. The figure reveals that the anisotropy essentially decays to lower long-time values going from Ω=0.4 to Ω=0.8 [panel (b)], whereas the redshift is not affected [panel (a)]. Thus, we can fit l_{seg} and Ω independently from the two experiments.

The *y* axis of the inset is the average probability of the excitons to hop up and down in energy. It can be seen that the downhill transfer probability decreases with time, whereas the uphill transfer probability increases. The corresponding transfer times are 6 ps at early times increasing to 25 ps in the long-time limit for downhill transfers. The reason for this nonexponential behavior is that the excitations easily find a low-energy segment with a high transfer probability at early time resulting in the short transfer times. In the long-time limit both probabilities are similar within the noise level of the plots. This indicates that thermal equilibrium is reached. Essentially, the hopping probability is nonzero and constant from this time on. This means that the excitation migrates at all times through thermally activated transfer steps, even when the spectral relaxation and anisotropy decay rate have reached their final value.

Since the spectral relaxation is intrinsically nonexponential and thus inhibits the quotation of time constants, we use the pairwise hopping time in order to make comparison to other publications possible.[43] It is defined as the inverse of the hopping probability between two isoenergetic conjugated segments with in-line configuration. For l_{seg}=2.9 nm the pairwise hopping time is 36 ps. This is somewhat slower than the 9–10 ps obtained by Grage *et al.* from fits of anisotropy decays of PDOPT (Ref. 22) and agrees well with findings by Hennebicq *et al.*, who use a modified Förster model based on quantum-chemical calculations to model spectral migration.[44]

In the following paragraph we will focus on the simulation of exciton migration on single polymer chains. Figure 4 shows the anisotropy and spectral shift averaged over 2500 excitons evolving on three chains. The orientation in the lab-frame was also kept constant. Panel (a) shows the three chain conformations, panels (b) and (c) present the spectral diffusion and anisotropy decay, respectively. Each exciton visits

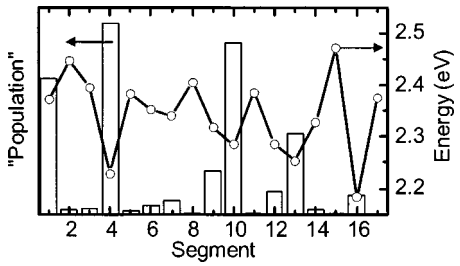

FIG. 5. Chain (ii) from Fig. 4 is examined in detail. The bottom axis is the number of the segment on the chain, the left-hand axis represents the time-integrated population (over 200 ps), and the right-hand axis is the energy associated with the segment.

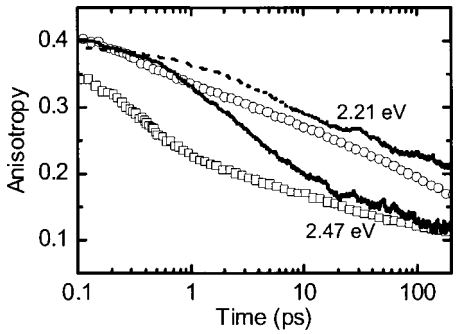

FIG. 6. Polarization anisotropy (FTA, detection at 1.96 eV) of PDOPT dissolved in chloroform with time after photoexcitation. Open squares and open circles are the experimental values for 2.47 and 2.21 eV excitation energy, respectively. The solid line (2.47 eV) and dashed line (2.21 eV) denote the simulated curves.

5 ± 5 (chain i), 4 ± 3 (ii), and 6 ± 4 (iii) segments during the time scale shown. The graphs highlight the distinct differences that occur between single chains: The anisotropy of the second chain (dashed curve) rises to 0.6 during 5 ps, which may indicate that the excitons transfer from a segment resonant with the excitation energy to another more in line with the excitation polarization. Another example highlighting the importance of microscopic conformation can be seen in the anisotropy of chain (iii). First it decays rapidly and then more slowly to negative values, indicating that the low-energy segments have a preferentially perpendicular orientation in respect to the excitation polarization.

Comparison to spectral relaxation data [panel (b)] reveals that the rapid changes in anisotropy occur as the excitons migrate mainly downhill in energy during the first 10 ps. This correlation between conformational and energetic disorder is mediated by incoherent energy transfer that is preferentially downhill and therefore fast at early times. The delicate interplay is highlighted in Fig. 5, which shows the time-integrated population probability and the energy of each segment of chain (ii). As expected, the low-energy segments have in general a larger population probability. However, the lowest energy segment ($n=16$) does not follow this trend. This site is less populated than the energy alone suggests. Excitons that are generated on the longer part of the chain are effectively blocked by the high-energy segment ($n=15$). The local conformation is thus important in determining the distribution of states occupied after spectral relaxation.

Of both experiments, anisotropy decay is potentially more sensitive to secondary processes like dynamic conformational disorder or intrasegmental dynamic localization.[14,45] Therefore, the hopping rate (controlled by means of l_{seg}) was determined by fitting the emission redshift, whereas $\Omega=0.8$ was determined by long-time fits of anisotropy at 2.47 eV excitation energy. Based on this set of parameters, Fig. 6 shows the anisotropy kinetics for blue and red excitation. The simulation reproduces the kinetics for 2.21 eV during all times, although with a small offset. However, at short times and 2.47 eV excitation energy the model overestimates the anisotropy, revealing an extra component which is not accounted for in our RET model. Notably, the component is much more pronounced for blue excitation.

V. DISCUSSION

The exciton migration model presented here is based on incoherent energy transfer. The assumptions leading to Fermi's golden rule clearly leave no room for coherent interactions. Our findings presented in Fig. 2 are consistent with the random walk picture that has previously been used by many authors to describe exciton migration in polymer films and solutions.[19,20,22–24]

Since the traditional point-dipole approach does not hold for short transfer distances and extended dipoles, an advanced algorithm is needed.[35] The line-dipole approximation is a candidate that has distinct advantages, notably that all parameters are easily experimentally available and that the computation time is fast. We note that quantum-chemical methods would be even more realistic, but require much more computational effort.[44,46] Even the "extended dipole model" published by Kuhn *et al.* would allow for a more realistic description of the interaction energies between two chromophores.[47] However, this model does not yield the length of the associated dipoles in a quantum-chemical sense and is therefore not suitable for the purpose of this investigation.

Figure 7 shows the hopping probability between two chromophores with length 2.9 nm, computed using Eq. (9). The x axis is the number of subsegments [l_d in Eq. (9)]. Since Eq. (9) converges to the traditional Förster formula for $l_d=1$, the first point of the plots in Fig. 7 represents the point-dipole approximation and is marked as stars. The two panels correspond to parallel (center-to-center distance 0.5 nm) and in-line configuration, respectively. The parallel configuration is important for interchain RET, whereas the in-line configuration is characteristic for the intrachain RET. In both cases the line-dipole approximation converges after a couple of subsegments. For parallel configuration the point-dipole approximation overestimates the hopping probability, whereas for the in-line approximation it underestimates it, in both cases by a factor of more than 10. Thus, the relative orientation of the chromophores is decisive in determining whether the point-dipole approximation under- or overestimates the Coulombic coupling. This agrees well with recent findings by Wiesenhofer *et al.*, who compare the point-dipole approximation to an improved Förster model that incorporates the shape of the excited state wave function by using atomic transition densities.[48] The observation should be carefully taken into account when discussing intra- vs interchain energy transfer in polymer films. In reality, the time scale of

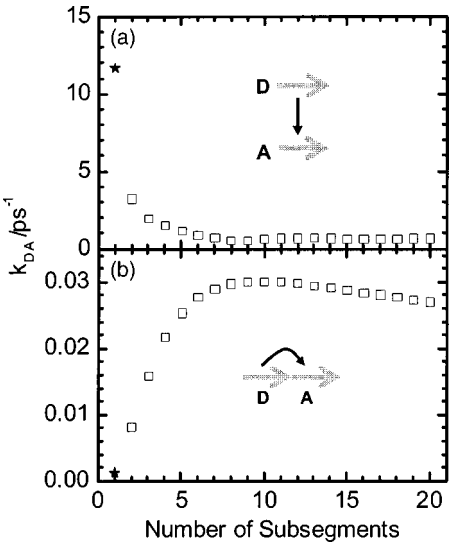

FIG. 7. Panel (a) shows the hopping probability [k_{DA}, Eq. (9)] between two chromophores oriented parallel to each other. The center-to-center distance is 0.5 nm and the chromophore length 2.9 nm. Panel (b) shows the hopping probability for in-line configuration of the chromophores (also 2.9 nm). The *x* axis represents the number of line-dipole subsegments [l_d in Eq. (9)]. The stars mark the values obtained for point-dipole approximation.

exciton migration along the chain may be underestimated and between the chains overestimated by more than an order of magnitude when the point-dipole Förster model is used.

The 1D wave function ($\Psi_{l,k}$) which is invoked in the line-dipole approximation can be expected to be a severe approximation. However, it is in principle possible to easily modify the shape of $\Psi_{l,k}$, i.e., to account for bridging molecules or difference in extent of the wave function in the ground- and excited states. We also performed simulations of exciton bimolecular dynamics based on the line-dipole approximation in molecular superassemblies that serve as model systems for intrachain energy transfer with very small interchromophore distances.[49] We find that the line-dipole approximation fails to work quantitatively and a correction parameter is needed to fit the data.[50] This may be because the 3D extension of a "real" wave function is rather more important in the case of interchain transfer between closely packed chromophores.

The fitted length of the chromophores of 7.4 monomers is slightly longer than the 6 monomers obtained by comparison to oligomer spectra.[22] Fits obtained via RET are far more sensitive to the chromophore length, because the hopping rate is proportional to $\sim r^{-6}$, while in the latter method the band gap is proportional r^{-1}. We note that the chromophore length we determine depends on the hopping distance and thus on the extend of ground- and excited state delocalization (whichever is larger). Since the excited state in conjugated polymers is more localized due to self-localization,[14,17] the larger conjugation length found in this RET study can be rationalized.

In order to assign the extra, non-RET component in the experimental anisotropy decay shown in Fig. 6, we will consider the following scenario. The energy of a particular segment is higher the more bent and twisted the chain is. Thus, hops away from segments with high energy result in a larger change of polarization than transfers between segments that are low in energy. This would explain the mismatch between experiment and model during the first 10 ps, because at early times high-energy segments are more likely to be populated. Furthermore, the extra component is not present when exciting the red edge of the absorption spectrum selectively. The scenario would explain this observation, because in the case of red excitation the high-energy segments are never populated significantly. Finally, the time scale on which the additional component plays a role ($\sim$10 ps) agrees well with the time at which the equilibrium between up- and downhill hops is established (Fig. 3, inset). Alternatively, the polymer chain could bend onto itself to form low-energy segments that are aligned with respect to each other. We note that due to the bulky sidechains of PDOPT, which are reported to cause reduced interchain contact in films,[33,38] it seems unlikely that this process takes place in solution, but this possibility cannot be excluded at this stage. Based on this scenario, we conclude that conformational disorder plays a vital part in limiting the effective conjugation in PDOPT.

As an alternative explanation it may be possible that additional processes which cause fast anisotropy decay but no significant spectral relaxation are active. Candidates are dynamic conformational disorder,[30,45] planarization of adjacent monomers,[31] and ultrafast processes such as intrasegmental self-localization.[14,17,23] The latter can be excluded as an explanation for the mismatch of the fits because they occur on the time scale of vibronic cooling ($<$100 fs) and should therefore not be observable in the experiments presented here.

Planarization after initial photoexcitation was proposed by Dias *et al.* to be responsible for the Stokes shift in solutions of a polyfluorene derivative on the picosecond time scale.[31] In the paper the authors also state that the effect is not seen in a more rigid derivative. Such a process would cause irreversible energy relaxation, but very little change of polarization since the main driving force, the gain of planarity, is not associated with a loss of polarization. Thus, the effects of planarization do not match well with the observations for PDOPT chains presented here. Absence of this component may be due to the bulky side chains of PDOPT that make a fully planar conformation unfavorable for steric reasons.

Within the concept of dynamic conformational disorder the exciton migrates as the monomers undergo random spatial and temporal fluctuations. This should lead to significant depolarization.[29] However, this process would not explain our observation that the extra, non-RET component is not present for site-selective excitation at the red edge of the absorption spectrum. Since dynamic conformational disorder is not intrinsically connected to the excited state, one would not expect a distinct dependence on excitation energy.

VI. CONCLUSION

We have used a Monte Carlo simulation to model exciton migration along conjugated polymer chains in solution. The line-dipole approximation was incorporated into the standard Förster formula, and we have shown that this model

quantitatively reproduces time-resolved anisotropy and PL spectral relaxation data at two excitation energies. The length of the conjugated segments and the conformational disorder of the chains were yielded directly as fitting parameters. The simulations reveal that the relaxed spectrum is determined by an equilibrium of up- and downhill transfers modulated by local conformational disorder. By comparing both experiments an additional component was identified in the anisotropy decay at blue excitation, which was qualitatively explained by conformational disorder limiting the effective conjugation length. High-energy segments are expected to be found in strongly bent parts of the chains, and a transfer away from those will result in significantly greater loss of polarization than hops between low-lying, relatively straight segments.

ACKNOWLEDGMENTS

The authors would like to thank Neil C. Greenham and Tönu Pullerits for helpful discussions and critical comments, as well as Mats Anderson for providing the polymer samples. S.W. thanks the Oppenheimer Fund for the studentship at Cambridge University; C.S. acknowledges financial support from the EPSRC via the Advanced Research Fellowship scheme. V.S. and A.Y. thank the Swedish Research Council and the Knut and Alice Wallenberg Foundation for financial support.

[1]R. H. Friend, R. W. Gymer, A. B. Holmes *et al.*, Nature (London) **397**, 121 (1999).
[2]C. J. Brabec, N. S. Sariciftci, and J. C. Hummelen, Adv. Funct. Mater. **11**, 15 (2001).
[3]H. Sirringhaus, N. Tessler, and R. H. Friend, Science **280**, 1741 (1998).
[4]H. Sirringhaus, T. Kawase, R. H. Friend, T. Shimoda, M. Inbasekaran, W. Wu, and E. P. Woo, Science **290**, 2123 (2000).
[5]T. Kawase, H. Sirringhaus, R. H. Friend, and T. Shimoda, Adv. Mater. (Weinheim, Ger.) **13**, 1601 (2001).
[6]N. C. Greenham, X. G. Peng, and A. P. Alivisatos, Phys. Rev. B **54**, 17628 (1996).
[7]M. Pope and C. E. Swenberg, *Electronic Processes in Organic Crystals and Polymers*, 2nd ed. (Oxford Scientific, New York, Oxford, 1999).
[8]U. Rauscher and H. Bässler, Macromolecules **23**, 398 (1990).
[9]T. Q. Nguyen, J. J. Wu, V. Doan, B. J. Schwartz, and S. H. Tolbert, Science **288**, 652 (2000).
[10]K. Pichler, D. A. Halliday, D. D. C. Bradley, P. L. Burn, R. H. Friend, and A. B. Holmes, J. Phys.: Condens. Matter **5**, 7155 (1993).
[11]Z. G. Zoos and K. S. Schweitzer, Chem. Phys. Lett. **139**, 96 (1987).
[12]G. D. Scholes, D. S. Larsen, G. R. Fleming, G. Rumbles, and P. L. Burn, Phys. Rev. B **61**, 13670 (2000).
[13]S. N. Yaliraki and R. J. Silbey, J. Chem. Phys. **104**, 1245 (1996).
[14]W. J. D. Beenken and T. Pullerits, J. Phys. Chem. B **108**, 6164 (2004).
[15]B. J. Schwartz, Annu. Rev. Phys. Chem. **54**, 141 (2003).
[16]J. Yu, D. H. Hu, and P. F. Barbara, Science **289**, 1327 (2000).
[17]S. Heun, R. F. Mahrt, A. Greiner, U. Lemmer, H. Bässler, D. A. Halliday, D. D. C. Bradley, P. L. Burn, and A. B. Holmes, J. Phys.: Condens. Matter **5**, 247 (1993).
[18]N. T. Harrison, D. R. Baigent, I. D. W. Samuel, R. H. Friend, A. C. Grimsdale, S. C. Moratti, and A. B. Holmes, Phys. Rev. B **53**, 15815 (1996).
[19]S. C. J. Meskers, J. Hubner, M. Oestreich, and H. Bassler, J. Phys. Chem. B **105**, 9139 (2001).
[20]R. Kersting, B. Mollay, M. Rusch, J. Wenisch, G. Leising, and H. F. Kauffmann, J. Chem. Phys. **106**, 2850 (1997).
[21]L. M. Herz, C. Silva, A. C. Grimsdale, K. Müllen, and R. T. Phillips, Phys. Rev. B **70**, 165207 (2004).
[22]M. M. L. Grage, T. Pullerits, A. Ruseckas, M. Theander, O. Inganäs, and V. Sundström, Chem. Phys. Lett. **339**, 96 (2001).
[23]M. M. L. Grage, P. W. Wood, A. Ruseckas, T. Pullerits, W. Mitchell, P. L. Burn, I. D. W. Samuel, and V. Sundström, J. Chem. Phys. **118**, 7644 (2003).
[24]M. M. L. Grage, Y. Zaushitsyn, A. Yartsev, M. Chachisvilis, V. Sundström, and T. Pullerits, Phys. Rev. B **67**, 205207 (2003).
[25]S. Haan and R. Zwanzig, J. Chem. Phys. **68**, 1879 (1980).
[26]J. Baumann and M. D. Fayer, J. Chem. Phys. **85**, 4087 (1986).
[27]G. Zumofen, J. Klafter, and A. Blumen, J. Chem. Phys. **79**, 5131 (1983).
[28]K. M. Gaab and C. J. Bardeen, J. Phys. Chem. B **108**, 4619 (2004).
[29]T. Palszegi, B. Mollay, and H. F. Kauffmann, J. Chem. Phys. **108**, 7023 (1998).
[30]E. N. Bodunov, M. N. Berberan-Santos, and J. M. G. Martinho, Chem. Phys. Lett. **340**, 137 (2001).
[31]F. B. Dias, A. L. Macanita, J. S. de Melo, H. D. Burrows, R. Güntner, U. Scherf, and A. P. Monkman, J. Chem. Phys. **118**, 7119 (2003).
[32]M. I. Sluch, A. Godt, U. H. F. Bunz, and M. A. Berg, J. Am. Chem. Soc. **123**, 6447 (2001).
[33]M. Theander, O. Inganäs, W. Mammo, T. Olinga, M. Svensson, and M. R. Andersson, J. Phys. Chem. B **103**, 7771 (1999).
[34]T. Förster, Ann. Phys. **2**, 55 (1948).
[35]W. J. D. Beenken and T. Pullerits, J. Chem. Phys. **120**, 2490 (2004).
[36]M. R. Andersson, T. Olinga, W. Mammo, M. Svensson, M. Theander, and O. Inganas, J. Mater. Chem. **9**, 1933 (1999).
[37]T. Wilhelm, J. Piel, and E. Riedle, Opt. Lett. **22**, 1494 (1997).
[38]K. E. Aasmundtveit, E. J. Samuelsen, W. Mammo, M. Svensson, M. R. Andersson, L. A. A. Pettersson, and O. Inganäs, Macromolecules **33**, 5481 (2000).
[39]S. Setayesh, D. Marsitzky, and K. Müllen, Macromolecules **33**, 2016 (2000).
[40]D. Beljonne, G. Pourtois, C. Silva, E. Hennebicq, L. M. Herz, R. H. Friend, G. D. Scholes, S. Setayesh, K. Müllen, and J. L. Bredas, Proc. Natl. Acad. Sci. U.S.A. **99**, 10982 (2002).
[41]J. G. Müller, U. Lemmer, G. Raschke, M. Anni, U. Scherf, J. M. Lupton, and J. Feldmann, Phys. Rev. Lett. **91**, 267403 (2003).
[42]G. D. Scholes, Annu. Rev. Phys. Chem. **54**, 57 (2003).
[43]T. Pullerits and A. Freiberg, Biophys. J. **63**, 879 (1992).
[44]E. Hennebicq, G. Pourtois, G. D. Scholes *et al.*, J. Am. Chem. Soc. (to be published).
[45]T. Palszegi and H. F. Kauffmann, J. Chem. Phys. **105**, 1702 (1996).
[46]B. P. Krueger, G. D. Scholes, and G. R. Fleming, J. Phys. Chem. B **102**, 5378 (1998).
[47]V. Czikklely, H. Försterling, and H. Kuhn, Chem. Phys. Lett. **6**, 207 (1970).
[48]H. Wiesenhofer, D. Beljonne, G. D. Scholes, E. Hennebicq, J. L. Bredas, and E. Zojer, Adv. Funct. Mater. **15**, 155 (2005).
[49]C. Daniel, L. M. Herz, C. Silva, F. J. M. Hoeben, P. Jonkheijm, A. Schenning, and E. W. Meijer, Phys. Rev. B **68**, 235212 (2003).
[50]C. Daniel, S. Westenhoff, F. Makereel *et al.*, Phys. Rev. B (to be published).